Microarchitecture Fabrication Process
of the Artificial Bone

Zhongzhong Chen[1], Cheng Li[1], Zhiqiang Jiang[2], Zhiying Luo[3]

1．College of Mechanical Engineering , Zhengzhou University , Zhengzhou , Henan 450001 , China

2．Department of Mechanical Engineering , Zhengzhou Institute of Aeronautics ,
Zhengzhou , Henan 450015 , China

3．The Second Internal Hospital of Zhengzhou University , Zhengzhou University ,
Zhengzhou , Henan 450002 , China

Abstract：By using bionic modeling and rapid prototyping technology, a novel system based on air-pressure jet solidification (AJS) technique is developed to fabricate porous microarchitecture of the artificial bone. Acting as transitional carrier of the bone implant, the porous scaffolds formed could provide proper porosity and interconnections for the growth of bone tissue and nutrient transport. This approach is better than traditional fabrication processes, because the latter methods cannot fabricate a microarchitecture with spatial bending micropores so as to satisfy biological requirements. [Life Science Journal. 2006;3(3):88−93] (ISSN: 1097−8135).

Keywords：rapid prototyping; scaffolds; air-pressure jet solidification

Abbreviations：AJS: air-pressure jet solidification; DS: denatured sucrose; FDM: fused deposition modeling; RP: rapid prototyping

1 Introduction

In the view of tissue engineering, the osteo-replacement tissue must have proper aperture and porosity for bone repair so as to accelerate bone regeneration. Moreover, it must serve as three-dimensional (3-D) template for initial cell attachment and subsequent tissue regeneration[1−3]. Conventional wisdom states that scaffolds should be designed to match healthy tissue morphological characteristics and have an interconnected pore network for cell migration and nutrient transport. Furthermore, the simulation design of the inter-connective architecture has a decisive effect on the activation of bone substitute. The traditional methods to fabricate scaffolds include polymer foaming technique, particulate-leaching, solid-liquid phase separation, textile technique and extrusion process, etc[4−10]. But with these methods, the bionic architecture similar in morphological characteristics to the inter-microstructure of the natural bone could not be ensured, which is essential to vascularization and tissue regeneration.

Based on the building principle of fused deposition modeling (FDM) in rapid prototyping (RP) technology, a new forming technique−AJS system is developed, which can build up the bone scaffolds with a novel fabrication material. The formed scaffold possesses an exterior mould exactly coincident with the replaced bone and interior porous architecture simulating the microstructure of the natural bone tissue. By filling self-setting calcium phosphate cement (CPC, a kind of biomaterial for bone substitute) and rhBMP (recombinant human bone morphogentic protein, a kind of growth factor) into the scaffolds, the fabricated scaffolds are dissolved with the solidification of CPC, and then the simulated interior microstructure is formed.

2 Materials and Methods

2.1 Fabrication material

A kind of fabrication material − denatured sucrose(DS) is developed to form the 3-D scaffolds. As a forming material, DS has proper plasticity, ductility and viscosity, so that the 3-D scaffolds can be built up and will not distort after solidification. Equally important, as an implantable biomaterial, DS has some proper histological performance and can be served as a biomaterial stabilizer of protein to maintain the activation of rhBMP.

2.2 AJS system

AJS system is designed to fabricate the artificial bone based on the layer-by-layer manufacturing principle of RP[11]. In the process, refined DS is fed into two controllable jets and melted into a semi-molten state by a heating system. Each jet has a

small nozzle on the tip, the diameter of the nozzle is 0.2 mm. Both jets are connected to an air compressor. Fine DS filament can be expressed through the nozzle by applying compressed air. Under the control of a computer, the on-off operation of the pressure air can be controlled by electromagnetic valves, then a 3-D working platform moves according to the processed data generated from the bionic modelling. So the filament is deposited layer-by-layer, and finally, a 3-D part is built in the areas defined by CAD model (Figure 1).
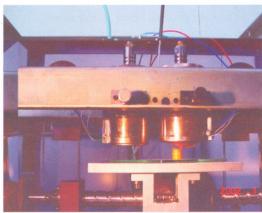

Figure 1. AJS system and its key part—two pressure jets

2.3 Diameter of filament

AJS system has many technical parameters, such as temperature of jet, squeezing and scanning velocity etc, all of these are the important process variables which determine the quality of the part. Due to the scaffolds fabricated, the key index is the diameter of filament in the fabrication process, which determine the configuration of the microarchitecture in the interior of artificial bone.

A calculation modeling is built up according to the matching relation of squeezing and scanning velocity of the jet. DS is a kind of thermoplastic material with a certain viscoelasticity. According to the viscoelastic and rheologic theory, it will keep in a semi-molten state in the whole fabrication process. Through double actions of air pressure and the traction force of the solidified layer, the shearing stress in DS would be occurred. Therefore, the tensile process is belong to non-Newtonia fluid and stretching flow. According to the theory analysis and expriments result, after the filament expressed from jet, the cross-section of filament can be concluded as Figure 2(a) in the tensile region, which is a rectangular CFGH (III) in the center and two conics at both ends.
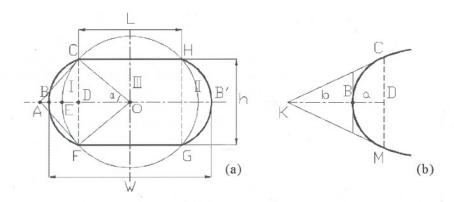

Figure 2. Illustration of solidification filament model in cross-section

According to the conic in Figure 2(b), line KC, KM are tangent to arc MBC, given MC = h ,

$KB = b$ and $BD = a$, ρ is defined as $a/(a + b)$, from spline geometrics, it can be educed that the contour of conic, namely the type of arc MBC can be determined by ρ, and a serial of conclusions could be derived as

1) $0.05 < \rho < 0.5$, the conic is ellipse;
2) $\rho = 0.5$, the conic is parabola;
3) $0.5 < \rho < 0.95$, the conic is hyperbola.

For easy to analysis and calculation, Figure 2 is simplified as follows:

a) While the squeezing velocity V_p is slow, namely while $\rho < 0.3$, the cross-section contour of filament can be simplified as rectangle Ⅲ in Figure 2(a). Due to the filament flow in unit time is equal to the forming volume required, an expression should be derived as

$$V_p \cdot \pi d^2/4 = V_s \cdot L \cdot h \qquad (1)$$

$$W = L = \frac{\pi d^2 V_p}{4hV_s} \qquad (2)$$

Where h is defined as the height between the nozzle and fabricated layer, d is the diameter of nozzle, V_p is the squeezing velocity, V_s is the scanning velocity of jet, L is the width of rectangle Ⅲ, W is the diameter of filament.

b) The area of conic must be taken into account while V_p is increased to a certainty. If the contour of conic is difficult to describe, arc FEC can be used for approximate the conic (Figure 2(a)). It belongs to the circle which include the four border point of rectangle Ⅲ, where O is defined as center of circle, segment AC, AF are tangent to arc CEP. Given $FD = DC = h/2$, $OD = L/2$, then the equation of ρ should be deduced as

$$\rho = \frac{ED}{BD} = \frac{\dfrac{\sqrt{L^2 + h^2} - L}{2}}{\dfrac{h}{L} \cdot \dfrac{h}{2}}$$

$$= [1 + \sqrt{1 + (\frac{h}{L})^2}]^{-1} \quad (0 < \frac{h}{L} < 1) \qquad (3)$$

While h/L is taken values in the interval of $(0, 1)$, according to expression (3), it can be concluded that variation range of ρ is in the interval of $(0.414, 0.5)$. Due to in the fabrication process, h/L is taken values in the interval of $(0, 0.5)$. Generally speaking, ρ is be in the interval of $(0.472, 0.5)$, namely ρ is set in the middle of value 0.05 and 0.95, therefore, the curvature range is between ellipse and hyperbola, which is approach parabola. Therefore, arc FEC is served as substitutional curve to calculate area I and Ⅱ approximately.

Therefore, while V_p is increased to a certainty, ρ is equal or greater than 0.3, the cross-section area of filament can be expressed as:

$$A_I = A_{sector(OFEC)} - A_{triangle(OPC)}$$

$$= \frac{1}{2}\left[\sqrt{\frac{L^2 + h^2}{2}}\right]^2 \cdot 2\alpha - \frac{L \cdot h}{4}$$

$$\approx \frac{1}{2}\left[\sqrt{\frac{L^2 + h^2}{2}}\right]^2 \cdot 2\frac{h}{\sqrt{L^2 + h^2}} - \frac{L \cdot h}{4}$$

$$(since \ \sin\alpha \approx \alpha, |\alpha| \ll 1)$$

$$= \frac{h}{4}(\sqrt{L^2 + h^2} - L) \qquad (4)$$

$$A_{section \ of \ filament} = A_{rectangle \ Ⅲ} + 2A_I$$

$$= L \cdot h + 2 \cdot \frac{h}{4}(\sqrt{L^2 + h^2} - L)^2$$

$$= \frac{h}{2}(\sqrt{L^2 + h^2} + L) \qquad (5)$$

From the principle of equal volume, it can be deduced that

$$\frac{\pi}{4}d^2 \cdot V_p = A_{section \ of \ filament} \cdot V_s$$

$$= \frac{h}{2}(\sqrt{L^2 + h^2} + L) \cdot V_s \qquad (6)$$

If $\zeta = \frac{\pi d^2 V_p}{2hV_s}$, it follows that

$$L = \frac{\zeta^2 - h^2}{2\zeta} \qquad (7)$$

In Figure 2(a), by using the length of segment AD as the distance of conic vertex to rectangular border CF, the value L can be deduced according to the expression (7), consequently, the expression of filament diameter can be derived

$$W = L + 2 \cdot AD = L + 2 \cdot \frac{h^2}{2L} = \frac{L^2 + h^2}{L} \qquad (8)$$

c) Illustration and analysis

In the fabrication process of filaments, given $d = 0.3 \ mm$, $h = 0.2 \ mm$, $V_p = 15 \ mm/s$, $V_s = 20 \ mm/s$, value W can be calculated from expression (2) and (8), which is 0.265 mm and 0.403 mm respectively. Comparing with the actual measurement result, which is 0.4 mm, it can be concluded that the calculation modeling of expression (8) is feasible, so that the calculation value is close to the actual result. Figure 3 shows the diameter variation of filaments in various processing parameter, for concreteness, $T = 115 \ ℃$, $P = 0.95 \ Mpa$, parameter h_k, V_s is variable.

2.4 Integrated fabrication

According to the bionic CAD modelling[12], some anatomical characteristic can be conclude that Haversian canals are connected by Volkmann's canals with a constant angle, the average diameter of Haversian canal is approximately 300 μm, the average diameter of Volkmann's canal is approximately 200 μm. In view of these considerations and the fabrication characteristic of AJS system, a

forming process can be designed to form conduction of osteons in one cross section by expressing the filament from point to point. Furthermore, in order to ensure the interconnection of osteons between upper and lower cross-sections, the jet should pause temporarily at the point of Haversian canals so that the filament can be expressed downwards further. In this way, the integrated fabrication of Haversian and Volkman's canals can be realized (Figure 4).
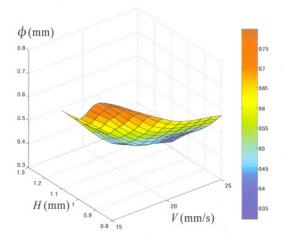

Figure 3. Diameter variation of filaments in various processing parameter
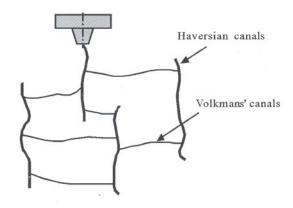

Figure 4. Schematic illustration of the microarchitecture forming process in vertical direction

From the mathematical model of the interior microstructure, the integrated fabrication of Haversian and Volkman's canals can be realized in the fabrication direction. After feeding DS into two jets, jet I and jet II are heated to 90 ℃ and 120 ℃ respectively and kept unchanged during the whole forming process. Jet I expresses fine filament with the platform moving in X-Y directions according to the processed data of exterior contour. After one layer of exterior contour is fabricated, the platform moves 0.2 mm downwards, and continues to fabri-

cate the next layer, so the exterior mould can be built up layer-by-layer. Until the required height reaches to build the interior scaffolds, jet I is cut off, and the platform moves horizonally to the position under jet II, then jet II begins to express fine filament. Therefore, in the whole process, with the platform moving according to the processed data, the fabrication of exterior mould and interior scaffolds can be built up by controlling the two jets cooperatively, so the 3-D scaffolds can be fabricated (Figure 5).
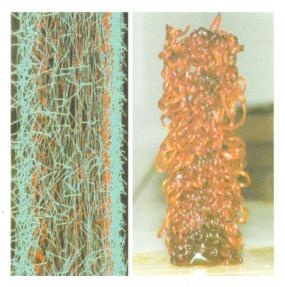

Figure 5. Simulated building of the interior 3-D scaffolds and corresponding scaffolds fabricated on AJS system

3　Results

3.1　Porous microstructure, porosity and pore dimension

After filling CPC into the cavities of bone scaffolds and solidifying process, the artificial bone can be produced. It can be concluded that the compressive strength of the bone substitute, the degradation rate and osteogenesis as well as osteogenetic quality are all associated closely with porosity. Equally important, the pore dimension is also a key index in osteoconduction, which plays an important role in infiltration of tissue fluid and osteogenesis. In view of medichine, the porosity of 60% or more and the pores dimension ranging from 200 to 500 μm in bone substitue are suitable for the bone regeneration[13]. The CPC porosity is 40%, and the average micropore dimension is about 5 μm. So the porous architecture of the bone scaffolds must include fabricated micropores and the inherent micropores of CPC. Therefore, the average diameters of Haversian canals and Volkman's canals should be controlled within 200 μm and 350 μm respectively.

The porosity can be adjusted by changing the height (H). Experiments determine that if fabricating two layer filament scaffolds within 1 mm, the interference or destruction between two adjacent filament scaffolds will occur, furthermore, the thermal field of the nozzle would melt the previous filament scaffolds. On the other hand, if fabricating two layer filament scaffolds to 4 mm or more, the interior architecture will distort and could not satisfy the necessary porosity. According to the experimental analysis, the suitable porosity can be well ensured if H is 2 mm, which can ensure the simulation accuracy and give enough space for heat dissipation.

The porous morphologies of the bone scaffolds are examined by gross observation, microscope and scanning electron microscopy (SEM). The bone scaffolds is cut off with a scalpel in both horizontal and vertical directions. Macroscopically, clear channels and micropores can be seen in both vertical and horizontal directions (Figure 6).

Under microscope (Keyence Company VH-8000, Japan), the porous morphologies encompassing Haversian canals and Volkman's canals are visible. There is no remarkable difference in shape or size between the filament scaffolds and the porous architecture formed in the bone scaffolds. The porosity of the bone scaffolds is 63.2% measured by toluene infiltration displacement method, which can satisfy the histological criterion of carrier scaffolds in bone tissue engineering.

The porous morphologies of the scaffold are examined by SEM at 20 KV (JEOL Company DJM-840, Japan) (Figure 7). From the energy spectrum analysis of line scanning between two micropores centers in a cross-section, it can be seen that there is no any chemical element in the center of micropore, the carbon content (the main element of DS) is the highest in the border of micropores, and decreases gradually outwards; at the same time, the content of calcium and phosphorus (the main elements of CPC) increase gradually. These findings suggest that micropores can be formed with the 3-D scaffolds of DS dissolving gradually during the solidification of CPC. So the validity of using filament scaffolds to fabricate the interior microstructure of bone scaffolds is confirmed.
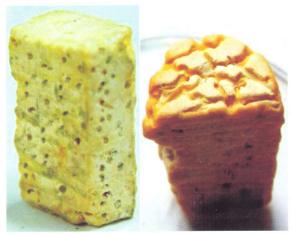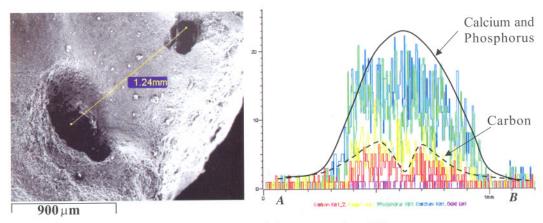

Figure 6. The fabricated bone scaffold

Figure 7. SEM image of the macropores in scaffolds

4　Conclusions

According to previous bionic CAD modelling for artificial bone, bone scaffolds can be produced through the fabrication system built and integrated fabrication method, which has the exact external contour of replaced bone and tissue-like 3-D scaffolds simulating the interior of natural bone. In this study, matching relation of processing parameters is determined through theory analysis and experiment, moreover, results show that some necessary

indexes of biology, such as porous microstructure, porosity and pore dimension can be obtained accurately, which can provide an inherent network of channels for tissue fluid circulation and realize bone transformation.

Correspondence to:
Zhongzhong Chen, Ph. D.
College of Mechanical Engineering
Zhengzhou University
Zhengzhou, Henan 450001, China
Telephone: 86-371-6778-1235
Email: zzchen@zzu.edu.cn

References
1. Sherwood JK, Riley SL, Palazzolo R, *et al*. A three-dimensional osteochondral composite scaffold for articular cartilage repair. Biomaterials 2002; 23(24): 4739 – 51.
2. Goldstein AS, Juarez TM, Helmke CD, *et al*. Effect of convection on osteoblastic cell growth and function in biodegradable polymer foam scaffolds. Biomaterials 2001; 22 (11): 1279 – 88.
3. Deng Y, Lin XS, Zheng Z, *et al*. Poly (hydroxybutyrate-co-hydroxyhexanoate) promoted production of extracellular matrix of articular cartilage chondrocytes *in vitro*. Biomaterials 2003; 24(23): 4273 – 81.
4. Vaz CM, van Tuijl S, Bouten CVC, *et al*. Design of scaffolds for blood vessel tissue engineering using a multilayering electrospinning technique. Acta Biomaterialia 2005; 1(5): 575 – 82.
5. Shum AWT, Li J, Mak AFT. Fabrication and structural characterization of porous biodegradable poly(dl-lactic-coglycolic acid) scaffolds with controlled range of pore sizes. Polymer Degradation and Stability 2005; 87(3): 487 – 93.
6. Ang TH, Sultana FSA, Hutmacher DW, *et al*. Fabrication of 3D chitosan-hydroxyapatite scaffolds using a robotic dispensing system. Materials Science and Engineering: C 2002; 20(1 – 2): 35 – 42.
7. Ma JB, Wang HJ, He BL, *et al*. A preliminary *in vitro* study on the fabrication and tissue engineering applications of a novel chitosan bilayer material as a scaffold of human neofetal dermal fibroblasts. Biomaterials 2001; 22 (4): 331 – 6.
8. Thomson RC, Mikos AG, Beahm E, *et al*. Guided tissue fabrication from periosteum using preformed biodegradable polymer scaffolds. Biomaterials 1999; 20 (21): 2007 – 18.
9. Lin ASP, Barrows TH, Cartmell SH, *et al*. Microarchitectural and mechanical characteri-zation of oriented porous polymer scaffolds. Biomaterials 2003; 24(3): 481 – 9.
10. Gomes ME, Godinho JS, Tchalamov D, *et al*. Alternative tissue engineering scaffolds based on starch: processing methodologies, morphology, degradation and mechanical properties. Materials Science and Engineering: C 2002; 20(1 – 2):19 – 26.
11. Hutmacher DW, Sittinger M, Risbud MV. Scaffold-based tissue engineering: rationale for computer-aided design and solid free-form fabrication systems. Trends in Biotechnology 2004; 22(7):354 – 62.
12. Petzold R, Zeilhofer HF, Kalender WA. Rapid prototyping technology in medicine-basics and applications. Computerized Medical Imaging and Graphics 1999; 23(5): 277 – 84.
13. Nakagawa T, Sugiyama T, Kamei T, *et al*. An immuno-light- and electron-microscopic study of the expression of bone morphogenetic protein-2 during the process of ectopic bone formation in the rat. Archives of Oral Biology 2001; 46(5): 403 – 11.